Heliyon 6 (2020) e04176

Contents lists available at ScienceDirect

Heliyon

journal homepage: www.cell.com/heliyon

Research article

Speculative analysis on the electronic structure, IR assignments and molecular docking of N-{4-[(4-amino-3-phenyl-1H-pyrazolo[3,4-d]pyrimidin-1-yl)sulfonyl]phenyl}acetamide, an anti-amoebic agent

Bindesh Kumar Shukla [a], Umesh Yadava [b,*]

[a] Department of Physics, SGS PG College, Ganj Basoda, Vidisha, 464221, India
[b] Department of Physics, DDU Gorakhpur University, Gorakhpur, 273009, India

ARTICLE INFO

Keywords:
Biophysics
Molecular physics
Theoretical chemistry
Pyrazolo[3,4-d]pyrimidine
Molecular electrostatic potential
HOMO-LUMO
IR assignment
Molecular docking
GAUSSIAN03
SCHRÖDINGER suite

ABSTRACT

An exhaustive quantum mechanical calculations on a pharmaceutically critical molecule N-{4-[(4-amino-3-phenyl-1H-pyrazolo[3,4-d]pyrimidin-1-yl)sulfonyl]phenyl}acetamide have been investigated through the B3LYP/6-31G** Density Functional and HF/6-31G** Wave Function techniques. Physicochemical parameters along with the advanced electronic structure parameters like; MEP (molecular electrostatic potentials) and highest occupied & lowest unoccupied molecular orbitals (HOMO-LUMO) analysis have additionally been scanned over both methods. The computed HOMO-LUMO energy demonstrates that charge exchange takes place inside the molecule. The estimated small HOMO-LUMO energy gap, through both methods, indicates that the molecule is chemically reactive. Further, the IR vibrational spectra of the molecule have been assigned in the region 400-4000 cm^{-1} through the DFT technique. The anticipated vibrational assignments have been compared with the experimental values accounted for in the literature. To comprehend the mode of binding, docking investigations of the molecule alongwith the co-crystallized metronidazole (MNZ) molecule were accomplished with O-acetyl-serine-sulfhydrylase (OASS) enzyme using GLIDE-SP and GLIDE-XP modules. Docking simulations and reported biological activities (IC50) demonstrate that the title molecule may act as a lead molecule for constraining the progression of *Entamoeba histolytica* illness.

1. Introduction

Amoebiasis, one of the most pouring reasons of the death from intestinal protozoan parasite *Entamoeba histolytica*, is a notable medical issue in the Third World Nations [1]. The situation influences over 10% of the total residents, and unprocessed contamination may prompt extreme inconveniences, including hepatic amoebiasis and intestinal tissue obliteration [2]. The *E. histolytica* causes about 50 million medical circumstances per year out of which around one million people die [3]. Usually, the luminal parasite is spread into the colon wall and beyond which can lyse and devastate the intestinal tissue and the amoebiasis is caused [4]. The *E. histolytica* genome provide the key understanding of this multistage process. There are enormous promise for the novel drug development using the metabolic and signaling pathways of the *Entamoeba histolytica* parasite [5]. Metronidazole (MNZ) is the mainline drug against amoebiasis, yet late examinations have demonstrated that this medication has a few dangerous impacts, such as, genotoxicity, gastric bodily fluid disturbance, and spermatozoid harm [6, 7]. Moreover, disappointments in the treatment of a few abdominal protozoan fleas may come about because of medication impervious to parasites [8, 9]. These issues impelled us to scan for new antiamoebic representatives. Pyrazolo[3–4,d]pyrimidine molecules are endowed with antiamoebic actions [10, 11, 12, 13], alongwith the inhibition of anti-coagulation and inflammation activities of viper PLA_2 [14], β-oxidation trifunctional enzyme of *Mycobacterium tuberculosis* [15] and other potential pharmaceutical activities [16, 17, 18]. Additionally, pyrazolo[3,4-d]pyrimidine compounds are the outstanding archetypal frameworks utilized for examining the intra- and intermolecular aromatic π-π interactions [19, 20]. These compounds have successfully proven to find applications in the treatment of thyroid carcinoma human cancers [20] also.The *in-vitro* antiamoebic activity of such a compound namely, N-{4-[(4-amino-3--phenyl-1H-pyrazolo[3,4-d]pyrimidin-1-yl)sulfonyl]phenyl}acetamide against HM1:IMSS strain of *Entamoeba histolytica*, demonstrates the

* Corresponding author.
E-mail address: u_yadava@yahoo.com (U. Yadava).

https://doi.org/10.1016/j.heliyon.2020.e04176
Received 7 April 2020; Received in revised form 6 May 2020; Accepted 5 June 2020

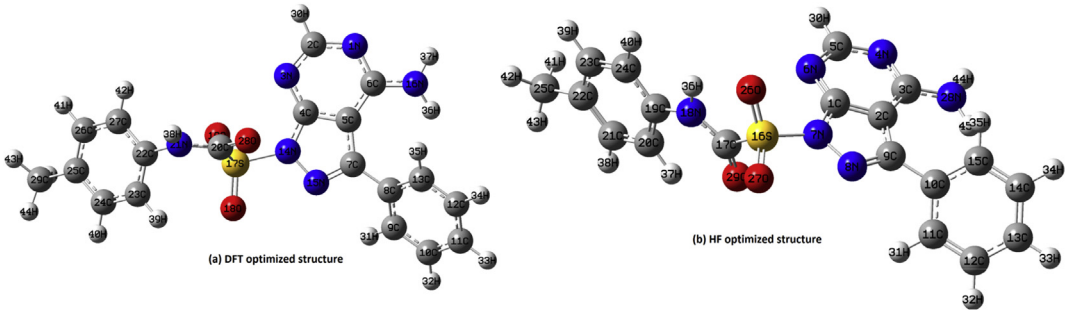

Figure 1. (a) DFT optimized and (b) HF optimized geometries of the N-{4-[(4-amino-3-phenyl-1H-pyrazolo[3,4-d]pyrimidin-1- yl)sulfonyl]phenyl}acetamide. (colour codes used for atoms: Blue-nitrogen, Red - Oxygen, Yellow: sulphur, Gray - Carbon, and Light gray - hydrogen).

better inhibitor action in contrast to the known drug metronidazole(MNZ) [13, 14].

In the present examination, electronic structure alongwith its physicochemical properties, HOMO-LUMO molecular frontier orbitals, molecular electrostatic potential (MEP) map, and spectroscopic assignments of the typical modes of the title molecule have been performed using Density Functional Theory and ab-initio Hartree-Fock wave function techniques. The results obtained through these quantum computational methods have been compared. The present inspection has been executed with a view purpose of vibrational frequencies analyzed and equated with experimental results as described in the literature [21]. Keeping in mind the end goal to think about the relative restricting affinities and noncovalent interactions, molecular docking investigations of the title molecule along with the co-crystallized drug metronidazole (MNZ) were done with the target O-acetyl serine sulfhydrylase (OASS) enzyme for hindering the development of *Entamoeba histolytica*. To guarantee accomplishment at the clinical trial level, we have also performed ADME (absorption, distribution, metabolism, excretion) forecast of the molecule through computations.

2. Methodology

2.1. Electronic structure calculation

The whole investigations were achieved at Hartree-Fock and Density Functional techniques in conjugation with the 6-31G** basis set utilizing the Gaussian-03 program package [22]. Both methods are established methods and can be used successfully in the case of small organic

Table 1. Comparison of bond lengths (Å), bond angles (°) and dihedral angles(°), computed through Gaussian-03 using Hartree-Fock(HF) and Density Functional (DFT) methods.

Bond length (Å)			Bond Angle ()			Dihedral angle ()		
Parameter	HF	B3LYP	Parameter	HF	B3LYP	Parameter	HF	B3LYP
N1–C2	1.335	1.341	N1–C2–N3	129.0	128.5	N1–C2–N3–C4	1.8	1.9
C2–N3	1.301	1.333	C2–N3–C4	112.8	111.8	C2–N3–C4–C5	1.6	1.9
N3–C4	1.332	1.336	N3–C4–C5	125.0	127.1	N3–C2–N1–C6	-2.2	-2.2
C4–C5	1.392	1.406	C2–N1–C6	117.7	118.3	N3–C4–C5–C7	179.4	178.0
N1–C6	1.319	1.344	C4–C5–C7	104.4	105.2	C4–C5–C7–C8	-179.5	-179.5
C5–C7	1.440	1.443	C5–C7–C8	130.2	130.0	**C5–C7–C8–C9**	**-138.0**	**-142.2**
C7–C8	1.482	1.476	C7–C8–C9	119.7	119.8	C7–C8–C9–C10	-179.0	-179.2
C8–C9	1.392	1.404	C8–C9–C10	120.4	120.4	C8–C9–C10–C11	0.0	-0.0
C9–C10	1.383	1.393	C9–C10–C11	120.3	120.3	C9–C10–C11–C12	0.4	0.7
C10–C11	1.386	1.397	C10–C11–C12	119.6	119.7	C10–C11–C12–C13	-0.3	-0.4
C11–C12	1.383	1.396	C11–C12–C13	120.2	120.2	C2–N3–C4–N14	-176.4	-177.9
C12–C13	1.386	1.396	N3–C4–N14	128.5	127.3	C4–C5–C7–N15	1.0	0.7
C4–N14	1.354	1.381	C5–C7–N15	109.9	110.6	C2–N1–C6–N16	179.6	179.2
C7–N15	1.284	1.322	N1–C6–N16	115.9	116.7	N3–C4–N14–S17	-8.4	-5.7
C6–N16	1.361	1.359	C4–N14–S17	130.1	127.9	**C4–N14–S17–O18**	**161.5**	**179.1**
N14–S17	1.727	1.737	N14–S17–O18	104.4	106.1	**C4–N14–S17–O19**	**36.1**	**46.9**
S17–O18	1.429	1.458	N14–S17–O19	104.0	106.8	**C4–N14–S17–C20**	**-81.4**	**-67.7**
S17–O19	1.429	1.457	N14–S17–C20	107.2	97.9	**N14–S17–C20–N21**	**5.0**	**167.3**
S17–C20	1.878	1.907	S17–C20–N21	110.9	114.9	**S17–C20–N21–C22**	**179.2**	**3.02**
C20–N21	1.279	1.351	C20–N21–C22	120.3	129.8	**C20–N21–C22–C23**	**-179.1**	**66.4**
N21–C22	1.394	1.436	N21–C22–C23	116.1	120.6	N21–C22–C23–C24	-180.0	178.0
C22–C23	1.400	1.396	C22–C23–C24	121.7	119.5	C22–C23–C24–C25	0.0	-1.2
C23–C24	1.378	1.394	C23–C24–C25	121.3	121.3	C23–C24–C25–C26	0.1	0.1
C24–C25	1.393	1.400	C24–C25–C26	117.1	118.1	C24–C25–C26–C27	-0.2	0.9
C25–C26	1.384	1.403	C25–C26–C27	122.3	121.1			
C26–C27	1.387	1.392						

Parameters having significant variations, as calculated through DFT and HF methods.

Table 2. Computed net partial atomic charges of N-{4-[(4-amino-3-phenyl-1H-pyrazolo[3,4-d]pyrimidin-1- yl)sulfonyl]phenyl}acetamide.

Atom No.	Atom	Atomic charge	
		HF	B3LYP
1	N	-0.671	-0.431
2	C	0.342	0.184
3	N	-0.560	-0.404
4	C	0.665	0.502
5	C	-0.266	-0.024
6	C	0.686	0.357
7	C	0.222	0.174
8	C	-0.029	0.081
9	C	-0.119	-0.091
10	C	-0.145	-0.093
11	C	-0.153	-0.078
12	C	-0.147	-0.095
13	C	-0.157	-0.145
14	N	-0.679	-0.519
15	N	-0.230	-0.254
16	N	-0.754	-0.597
17	S	1.601	1.239
18	O	-0.670	-0.493
19	O	-0.666	-0.483
20	C	0.460	0.317
21	N	-0.703	-0.535
22	C	0.244	0.172
23	C	-0.166	-0.056
24	C	-0.133	-0.132
25	C	-0.049	0.135
26	C	-0.141	-0.129
27	C	-0.184	-0.067
28	O	-0.660	-0.394
29	C	-0.332	-0.377
30	H	0.147	0.109
31	H	0.187	0.116
32	H	0.141	0.095
33	H	0.135	0.091
34	H	0.138	0.092
35	H	0.176	0.110
36	H	0.307	0.276
37	H	0.308	0.283
38	H	0.132	0.292
39	H	0.105	0.124
40	H	0.109	0.093
41	H	0.192	0.089
42	H	0.104	0.101
43	H	0.104	0.115
44	H	0.108	0.116
45	H	-0.167	0.135

molecules [23]. We have used these two methods for the comparative examinations of the electronic structure performances on the molecule under study. The geometries were first decided using the Hartree-Fock method, after that, compared with the values obtained by DFT utilizing the Becke's three-parameter hybrid functional joined with Lee-Yang-Parr correlation functional strategy(B3LYP) [24]. The enhanced structural parameters were utilized as a part of the vibrational IR frequency(velocity of light in vacuum times wave number) calculations at DFT levels to portray the standing point as least. The optimized geometries were exploited to figure out all the physicochemical parameters alongside harmonic vibrational wave numbers of the selected molecule. The HOMO- LUMO and molecular electrostatic potential (MEP) surfaces of the improved structures have likewise been examined [25].

2.2. Molecular docking

The DFT optimized geometry of the title molecule alongwith the reference medicate metronidazole (MNZ) has been prepared utilizing the LIGPREP module of the Schrödinger Suite to adjust the bond orders as per their information and, diverse conformers were created utilizing CONFGEN. These prepared ligands were utilized for ligand docking. The 3-D structure of the target OASS (PDB ID: 4IL5) [26] was

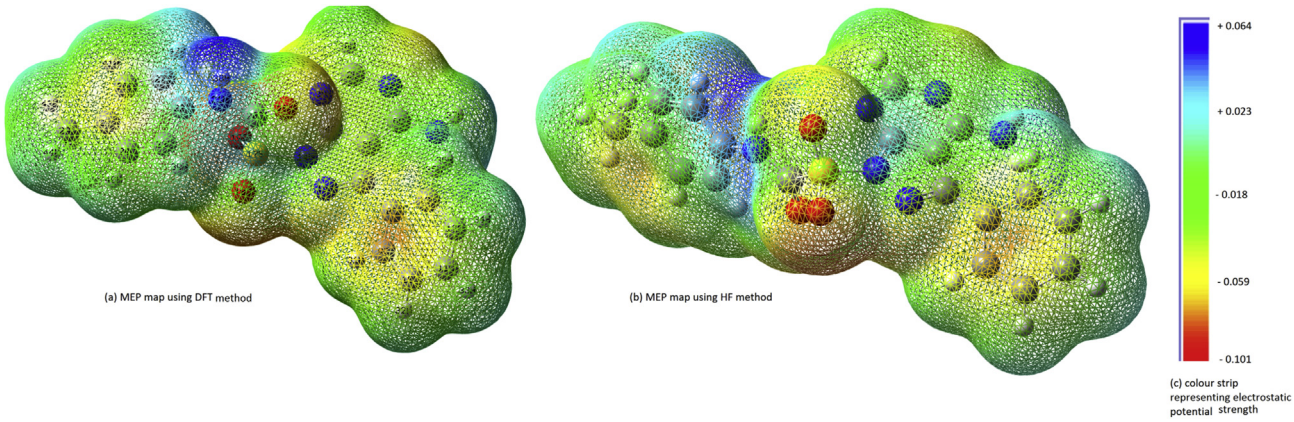

Figure 2. The molecular electrostatic potential using (a) density functional and (b) Hartree- Fock methods of the N-{4-[(4-amino-3-phenyl-1H-pyrazolo[3,4-d]pyrimidin-1- yl)sulfonyl]phenyl}acetamide molecule projected on the 0.001 electrons/bohr^3 isodensity surface. (c) colour strip representing the strength of electrostatic potential (Red color represents the regions of negative electrostatic potential, blue ones represent regions of positive electrostatic potential and white colour represents regions of zero potential).

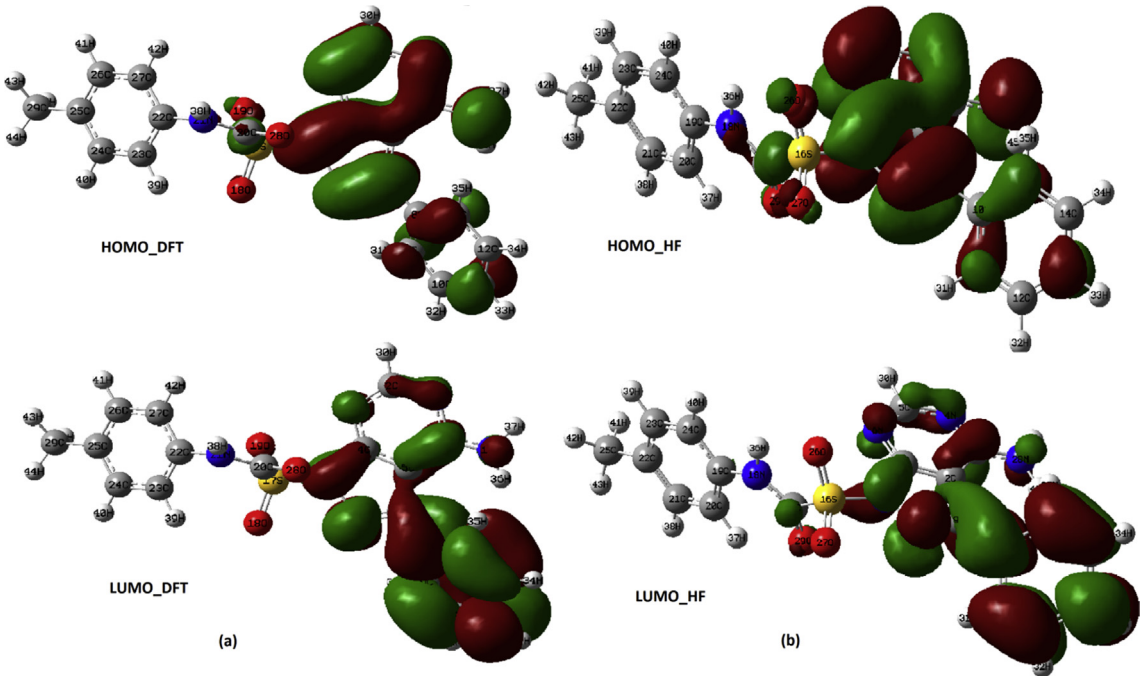

Figure 3. HOMO and LUMO of N-{4-[(4-amino-3-phenyl-1H-pyrazolo[3,4-d]pyrimidin-1- yl)sulfonyl]phenyl}acetamide molecule using (a) density functional method and (b) Hartree-Fock method. (The orbital wave functions are positive in the red regions and negative in the blue region).

downloaded from Protein Data Bank (http://www.rcsb.org/); which was prepared utilizing protein preparation wizard of the suite, to beat the assortment of potential issues, e.g. chain breaks, included water molecules, bond orders, missing residues, and so forth. The affinity and electrostatic potential grid were ascertained for each kind of atom in ligands at various grid points at the active site of the receptor. The location of MNZ remained the center of the active site. The docking calculations of prepared ligands were performed in the Standard precision (SP) and Extra precision (XP) modes of the GLIDE [27]. During docking, the target macromolecule was held fixed while ligands were dealtwith as flexible. Full force field minimization of those poses which were considered for the last scoring was accomplished. The outcomes were utilized for binding energy calculations and docking scores.

3. Results and discussion

3.1. Molecular geometry

In the present investigation, the optimized geometries in gaseous state of the title compound using B3LYP (density functional theory) and Hartree-Fock (wave function theory) strategies in conjugation with the standard 6-31G** basis set are depicted in Figure 1. The imperative bond lengths, bond angles, and dihedral angles, as obtained through both techniques have been compared and are displayed in Table 1. The calculated net Mulliken charges on every atomic center have been presented in Table 2. It is inspected that the processed geometrical parameters viz; bond lengths, bond angles, and dihedral angles acquired from both techniques are similar for core-ring regions while there are some

Table 3. The total energy, HOMO and LUMO energies of the N-{4-[(4-amino-3-phenyl-1H-pyrazolo[3,4-d]pyrimidin-1- yl)sulfonyl]phenyl}acetamide.

Parameters	HF	B3LYP
Total energy E (Hartree)	-1677.018	-1685.958
Dipole moment (Debye)	5.8623	1.1706
HOMO (Hartree)	-0.15490	-0.31556
LUMO (Hartree)	0.18647	0.08804
HOMO-LUMO energy gap (Hartree)	0.34137	0.4036

variations in the conformation of substituents. The most change in the conformation is at the sulfonyl site. The dihedral angles C4–N14–S17–O18 and C4–N14–S17–O19 calculated using HF/6-31G** method are 161.5° and 36.1° respectively which, after optimization through DFT/6-31G** change to 179.1° and 46.9°. Torsions N14–S17–C20–N21, S17–C20–N21–C22 and C20–N21–C22–C23 have also significant variations. These variations may be caused due to the presence of the sulphur atom, which exhibits different ionization states. As obvious from Table 2, all hydrogen atoms have acquired small positive charge irrespective of their position in the molecule. Atoms like nitrogen, oxygen, and sulfur consistently possess partially negative charges, while carbon atoms undertake both positive and negative charges contingent with their position in the molecule. The ascertained geometric parameters of the molecule can be utilized for the establishment of alternate parameters. The global least energies of the optimized structures as calculated through B3LYP/6-31G** and HF/6-31G** methods are -1685.958 Hartree and -1677.018 Hartree respectively.

3.2. Molecular electrostatic potential (MEP) and HOMO-LUMO analysis

Molecular electrostatic potentials (MEP) are important parameters that are utilized in order to observe molecular interactions [28]. The MEPs have been explored utilizing astounding wave function through B3LYP and Hartree Fock (HF) techniques at the self-consistent field level. The MEP surface of N-{4-[(4-amino-3-phenyl-1H-pyrazolo[3,4-d] pyrimidin-1-yl)sulfonyl]phenyl}acetamide on the 0.002 electron/bohr^3 isosurface density is shown in Figure 2. It is observed that electron densities are low at the exterior portion and close to hydrogen molecules (blue and light blue regions). Consequently, electrostatic potential around these regions is positive. Comparatively higher electron densities (yellow and green regions) are observed in the interior portion of the molecule, because of the proximity of the less electronegative carbon atoms. The electron densities are high close to the strong electronegative atoms like oxygen and nitrogen, the result is that the MEP scan exhibits negative potential destinations on oxygen and nitrogen atoms while positive potential locales are around the hydrogen atoms.

The HOMO and LUMO of the studied molecule as ascertained by B3LYP/6-31G** and HF/6-31G** techniques are displayed in Figure 3. The HOMO of the molecule is exceptionally fixated on phenyl rings including carbon atoms while less focused on the oxygen and nitrogen atoms. Partial charges on nitrogen atoms indicate the overlap of nitrogen atoms on the adjacent carbon atoms, which shortens the bond length between these atoms. The C–N group is likewise exceedingly controlled. In LUMO, the delocalization of valence (virtual) orbitals all through the atom has ensued. Nitrogen atoms of the bond assemble overlap each other and carbon atoms of the central linkage cover adjoining carbon atoms of the phenyl rings. Since phenyl rings are nearly co-planar, both HOMO and LUMO are proportioned. The aggregate electronic energy, dipole moment, HOMO, and LUMO energies and energy gap (ΔE) for the molecule are presented in Table 3. A molecule with a smaller energy gap is expected to have higher reactivity and lower stability in the chemical process with electron exchange or leap [23, 29]. It is seen from Table 3, the HOMO-LUMO energy gap is 0.4036 Hartree through the B3LYP strategy and 0.3414 Hartree through the HF method, which is diminutive and demonstrates that the molecule under study is synthetically reactive.

Table 4. Theoretically computed thermodynamical parameters of N-{4-[(4-amino-3-phenyl-1H-pyrazolo[3,4-d]pyrimidin-1- yl)sulfonyl]phenyl}acetamide.

Thermodynamical Parameters	DFT		HF
Zero-Point vibrational energy(kcal/mol)			
	211.505	218.683	
Rotational temperature (Kelvin)			
	0.017		0.009
	0.004		0.005
	0.003		0.004
Rotational constants(GHA)			
	0.348		0.267
	0.079		0.089
	0.070		0.079
Energy (kcal/mol)			
Total	227.331		239.405
Transtational	0.889		0.889
Rotatinal	0.889		0.889
Vibrational	225.553		237.465
Molecular Capacity at constant volume(cal/mol-kelvin)			
Total	96.026		87.324
Transtational	2.981		2.981
Rotatinal	2.981		2.981
Vibrational	90.064		81.362
Entropy (cal/mol-kelvin)			
Total	178.585		173.318
Transtational	43.910		43.903
Rotatinal	36.363		36.402
Vibrational	98.312		93.013

Table 5. Vibrational assignments of fundamental wave numbers for N-{4-[(4-amino-3-phenyl-1H-pyrazolo[3,4-d]pyrimidin-1- yl)sulfonyl]phenyl}acetamide at B3LYP/6−31G** level.

Experimental wave numbers (cm^{-1})	Theoretical wave numbers (cm^{-1})	Intensity (km/mol)	Vibrational assignments
411	424.02	11.375	Ring out of plane deformation
	425.11	0.084	
	436.10	45.404	
	466.45	22.710	
474	509.98	15.757	C–H out of plane bending
527	537.72	29.734	
551	553.72	9.581	
637	63173	1.826	
	651.69	30595	
693	694.78	32.962	CCC out-of-plane bending
	715.86	35.309	
776	775.87	26.379	C–H out of plane deformation
807	793.43	3.038	
824	826.19	11.240	
	834.39	28.614	
	845.45	1.549	
885	870.36	1.259	CH3 Rocking
1003	1004.26	0.368	Inter ring C–C stretching
1019	1016.24	0.506	C–C stretching
1061	1065.55	7.363	
1121	1121.57	193.653	In-plane ring HCC bending
1179	1182.14	182.655	
1215	1221.09	22.67	C–H in-plane bending
1265	1229.42	25.080	
	1237.70	8.582	
1306	1321.00	40.786	N–N stretching
1339	1336.41	18.929	C–N stretching
	1354.16	39.119	
	1359.07	88.426	
	1364.31	3.300	
	1376.90	19.203	
1466	1464.65	8.394	C–C Stretching
1478	1484.62	4.568	
	1501.37	4.940	
	1506.73	6.774	
1674	1667.29	0.154	NH_2 Scissoring
3032	3043.14	25.575	Aromatic C–H stretching
3070	3104.00	18.829	
3125	3130.25	13.563	
	3183.76	27.761	
	3186.06	12.611	
	3190.10	12.871	
	3192.40	7.209	
	3201.46	19.031	
	3209.53	19.632	
	3220.76	4.462	
	3226.79	0.728	
3472	3569.44	47.942	NH_2 asymmetric stretching
	3599.99	84.400	NH_2 symmetric stretching

3.3. Thermodynamical parameters

A few thermodynamic properties like heat capacity, zero-point vibrational energy, entropy alongside the global least energy of the title compound as acquired by *ab-initio* Hartree Fock and Density Functional Theory strategies utilizing B3LYP/6-31G** are presented in Table 4. The distinction in the values figured out by both strategies is just minimal. Scale factors have been suggested for an exact forecast in deciding the zero-point vibrational energy, and the entropy. The variations in zero-point vibrational energy is by all accounts insignificant [30]. The aggregate energy and the adjustment in the aggregate entropy at room temperature are additionally exhibited. As obvious from Table 4, as the rotational temperature changes, rotational constants likewise change. The rotational constant declines with the reduction in rotational temperature. The rotational constant is inversely related to the moment of inertia of the molecule. Hence, decrease in rotational constant demonstrates increment in the moment of inertia of the molecule.

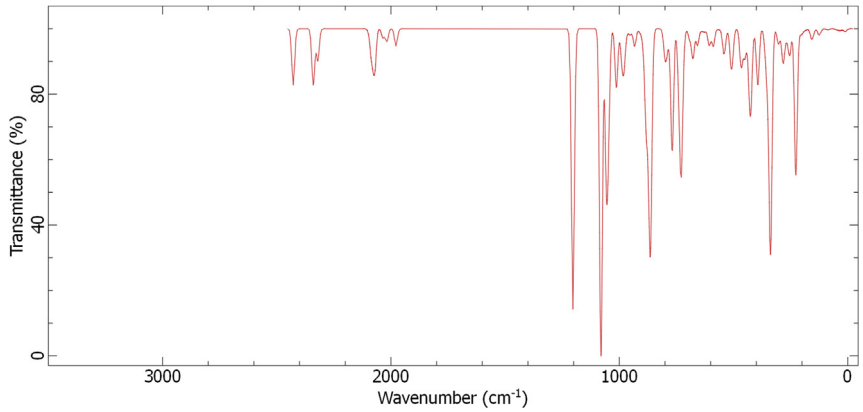

Figure 4. IR spectrum of N-{4-[(4-amino-3-phenyl-1H-pyrazolo[3,4-d]pyrimidin-1- yl)sulfonyl]phenyl}acetamide as observed from B3LYP/6-31G** method.

Table 6. Glide scores and average van der Waals (E_{vdw}), electrostatic (E_{coul}) and Glide energies as obtained through Glide SP and XP docking.

Compound	Glide Score (kcal/mol)		Evdw (kcal/mol)		Ecoul (kcal/mol)		Glide Energy (kcal/mol)		IC 50 (μg/ml)
	SP	XP	SP	XP	SP	XP	SP	XP	
Title molecule	-6.839	-5.463	-43.046	-43.074	-6.955	-6.996	-50.001	-50.070	0.68
MNZ	-4.217	-4.171	-20.192	-19.569	-5.159	-8.193	-25.351	-27.763	1.80

3.4. Vibrational analysis

Vibrational spectroscopy has noteworthy contributions towards the investigations of the structure and physicochemical properties of crystals and molecular systems. The vibrational examination of a picked compound has been made utilizing FTIR spectroscopy. An attractive assignment of the fundamental vibrations has been made by the position, shape, nature, and relative intensity. The vibrational IR spectra of N-{4-[(4-amino-3-phenyl-1H-pyrazolo[3,4-d]pyrimidin-1-yl)sulfonyl]phenyl} acetamide molecule in the region 400-4000 cm^{-1} comprises of vibrations characteristics of pyrazole and pyrimidine moieties, alkyl chains, CH and CN stretching modes, etc. Theoretically predicted vibrational (IR) frequencies of the molecule have been compared with the experimental observations and are introduced in Table 5, while the related spectrum is depicted in Figure 4.

3.4.1. The C–H vibrations

The C–H stretching vibrational modes of the aromatic and heteroaromatic structures occur in the wave number region 3000-3200 cm^{-1} [31]. The C–H stretching vibrations of N-{4-[(4-amino-3--phenyl-1H-pyrazolo[3,4-d]pyrimidin-1-yl)sulfonyl]phenyl}acetamide are predicted at 3043.14, 3104.00, 3130.25, 3183.76, 3186.06, 3190.10, 3192.40, 3201.46, 3209.53, 3220.76, 3226.79 cm^{-1} in the FT-IR spectra, while experimentally they are found at 3032, 3070, and 3125 cm^{-1}. The CH in-plane bands seen at 1221.09, 1229.42, 1237.70 cm^{-1}, with CH out-of-plane bending, were observed to be well inside the evocative region. The small differences in the wave numbers may be because of calculations in gaseous state of the molecule while reported experimental values are in solid states. Several values of the same type of vibrations represent their presence in different chemical environments.

3.4.2. The C–N vibrations

The unconjugated C–N linkage in the amine group offers average to weak groups close to 1250–1020 cm^{-1} as a result of C–N stretching vibration [32]. The IR groups seen at 1336.41, 1354.16, 1359.07, 1364.31, and 1376.90 cm^{-1}, are in the great concurrence with the experimentally observed values (1339 cm^{-1}). The slight distinction in wave number is because of the way the force constants of the C–N band expanded due to resonance with the ring.

3.4.3. C–C stretching vibrations

The vibrational band between 1400-1650 cm^{-1} is assigned to carbon-carbon vibrations. The FT-IR groups predicted at 1464.65, 1484.62, 1501.37, 1506.73 cm^{-1} are allocated to C–C extending vibrations, which are in agreement with the probing esteems of 1466, 1478, 1677 cm^{-1}. The normal mode for interring C–C stretching is observed at 1004.26 cm^{-1}, while experimentally it is found at 1003 cm^{-1}.

3.4.4. Ring vibrations

For the title molecule, the bands seen at 1121.57, 1182.14, and 1188.34 cm^{-1} in FT-IR are credited to ring in-plane bending types, while experimentally they are seen at 1121 and 1179 cm^{-1}. The twisting mode frequencies due to ring out-of-plane vibrations are observed at 424.02, 425.11, 436.10 cm-1, while experimentally they are found at 411cm^{-1}.

Table 7. Hydrogen bonding and other non-covalent interactions in the docked complexes of the ligands with OASS enzyme as obtained through Glide dockings.

Compounds	Hydrogen bondings	Hydrophobic interactions	Polar interactions	Other interactions
SP docking				
Title molecule	GLN235, ASN88, THR85, GLN159	MET112, TYR313, ALA239, PHE241, MET136, PRO137, ILE140	SER113, THR89, SER86, SER84	PHE60(Cation ...π)
MNZ	SER86, ASN88, LLP58, GLN159, GLY236	MET136, PHE160, ILE237, ALA239	THR85, THR89, THR193	LLP58(Cation ...π)
XP Docking				
Title molecule	GLN235, ASN88, THR85, GLN159	MET112, TYR313, ALA239, PHE241, MET136, PRO137, ILE140	SER113, THR89,SER86, SER84	PHE60(Cation ...π)
MNZ	THR85, THR89, LLP58, GLY236	MET136, PHE160, ILE237, ALA239	GLN159, THR85, SER86, ASN88, THR193	LLP58(Cation ...π) LLP58(Salt bridge)

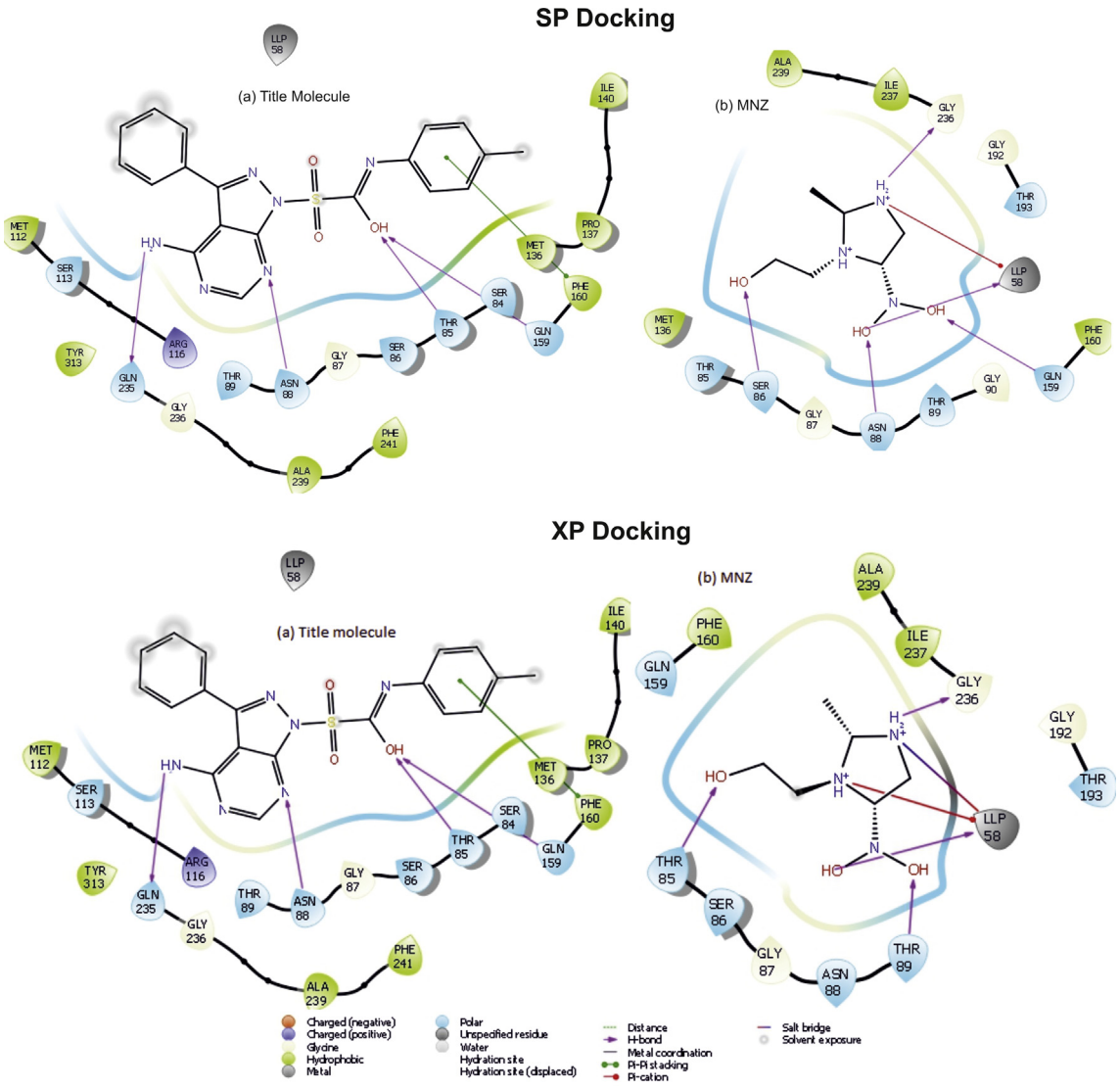

Figure 5. Hydrogen bonding and other non-covalent interactions in the best docking poses of the title molecule and MNZ as obtained through SP and XP docking protocols of Glide.

3.4.5. *Amino group vibrations*

Generally, the wave numbers of amino groups show up in the region 3300-3500 cm^{-1} for N–H stretching, 1600-1700 cm^{-1} for NH_2 scissoring, and 900-1150 cm^{-1} for rocking distortion. For the examined molecule asymmetric and symmetric extending vibrations are assigned out at 3569.44 and 3599.99 cm^{-1}respectively. NH_2 is assigned at 1674 cm^{-1}.

3.5. *Molecular docking simulation*

The estimation of different energy terms viz; Glide energy, van der Waal energy, Coulomb energy, and so on and Glide-score as acquired through standard precision (SP) and Extra Precisions (XP) protocols of Glide, along with the experimentally reported IC50 activities, are presented in Table 6. Docking of the title molecule with O-acetyl Serine Sulfhydrylase (OASS) compound uncovered an enormous variation in their binding energies. Even though the ascertained free energy of binding is a productive descriptor of ligand-receptor complementarities, the choice of the "best" docking model was at least articulated by an assortment of parameters of ADME study. It has been seen through SP docking that the title molecule has the best G-score (-6.839 kcal/mol) contrasted with reference medicate metronidazole (MNZ) (-4.217 kcal/mol). In the XP module of GLIDE, protein-ligand structural motifs promoting improved binding affinity were incorporated into expansion to one of a kind water destruction energy terms. The Glide docking after-effects of the XP protocol also revealed the title molecule with the highest docking score (-5.463 kcal/mol) compare to the reference drug metronidazole (- 4.171 kcal/mol). Glide energies for title molecule were more negative (-50.001 kcal/mol) than the reference medicate metronidazole. Several non-covalent interactions of the ligands with the residues of the active site, similar to hydrogen bonding, aromatic π-π stacking, and hydrophobic interactions, are observed. As obvious from Table 7, Figure 5, and Figure 6, the title molecule display four numbers of hydrogen bonding interactions through both protocols of the docking with residues GLN235, ASN88, GLN159, THR85, while the reference drug metronidazole indicate five number of hydrogen bonds with residues SER86, ASN88, GLN159, GLY236 and LLP58 through SP-docking while four number of hydrogen bonds involving residues THR85, GLY236, TH89 and LLP58 by XP docking. Aromatic π-π interaction is

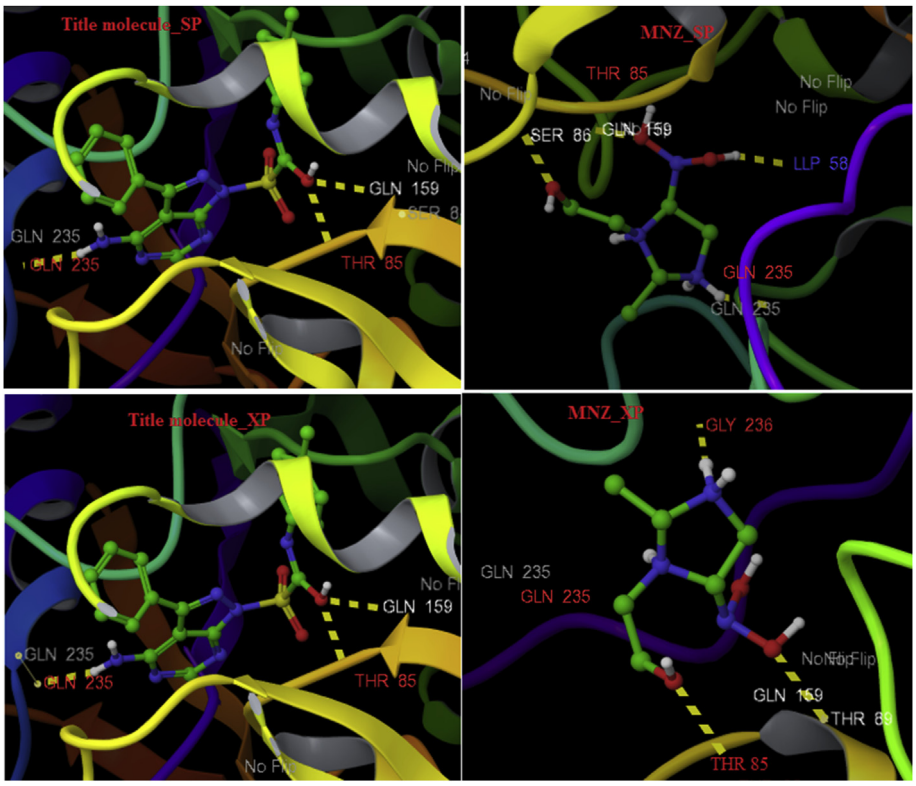

Figure 6. Hydrogen bonding interactions in the best docking poses of the title molecule and MNZ as obtained through Glide-SP and Glide-XP docking.

Table 8. ADME properties of the title molecule and metronidazole ((MNZ).

Properties	Log P	M. W.	nON	nOHNH	nRotb	PSA	Volume	Abs.	nViol.
Title molecule	25.391	408.434	10.500	3.000	4	136.493	1192.941	72.267	1
MNZ	25.405	444.424	11.700	3.000	8	173.486	1207.119	41.683	1
Range of 95% drugs	-2.0 to 6.5	130 to 725	2.0 to 20	0.0 to 6.0	0.0 to 15.0	7.0 to 200.0	500 to 2000	>25%	0–4

exhibited by the title molecule with the residue Phe160. The MNZ, within binding site, exhibit cation-π and salt bridge interactions with LLP58. Binding site residues MET112, TYR313, ALA239, PHE241, MET136, PRO137, ILE140, PHE160, ILE237, ALA239 etc form hydrophobic enclosure while SER113, THR89, SER86, SER84, THR85, THR193, GLN159, etc. are responsible for polar interactions. Estimations show that the title molecule has a better binding capability with O-acetyl Serine Sulfhydrylase enzyme against *Entamoeba histolytica* as compared to the established drug metronidazole (MNZ).

3.6. ADME property

ADME properties figured out utilizing QikProp3.5 [33] anticipated 44 properties for title molecule, comprising of primary descriptors and physicochemical properties. Adequacy of the analogs in light of "Lipinski's rule of five" is additionally computed, which is fundamental for a reasonable medication plan. It has been observed that the title molecule and the reference drug MNZ both exhibit one violation of the Lipinski's rule of '5′(Table 8). The voilation of more than one or two rules of '5′ may have issues with bioavailability. ADME estimations and docking simulations come about to assign that the considered molecule might be developed as a lead compound as the inhibitor of the OASS enzyme.

4. Conclusion

An attempt has been made in the present investigations to analyzed molecular geometry, HOMO-LUMO, MEP surface and vibrational spectra of N-{4-[(4-amino-3-phenyl-1H-pyrazolo[3,4-d]pyrimidin-1-yl)sulfonyl] phenyl}acetamide molecule utilizing Density Functional theory (B3LYP/6-31G**) and wave function theory (HF/6-31G**) methods. The parameters (bond length and bond angle) of the optimized geometry figured through both HF and B3LYP strategies in conjugation with a 6-31G** basis set are observed to be in great concurrence with each other. However, variations have been observed in the conformations of the molecule at the sulfonyl site. MEP indicates that electrophilic ability reinforces besides nucleophilic capacity deteriorates as one moves away from the internal center of the molecule. The calculated HOMO and LUMO energies demonstrate that possible charge exchange happens inside the molecule, and little value of the HOMO-LUMO gap demonstrated that the title molecule is chemically reactive. The total vibrational assignment of wavenumbers is made on the premise of aggregate energy distribution. The computed vibrational frequencies were found in great harmony with the experimental results accessible in literature. The DFT optimized geometry of the molecule has been used for docking within binding site of the OASS enzyme of the *Entamoeba* Histolytica. The partial charges demonstrated by MEP map helped in the creation of affinity grid

map during docking. Molecular docking simulation and ADME property estimations demonstrate that the title molecule has a better binding ability with the target OASS than the reference medicate metronidazole (MNZ), which are very similar to those of experimentally reported biological IC50 values for inhibiting the development of amoebiasis due to *Entamoeba histolytica*.

Declarations

Author contribution statement

Umesh Yadava: Conceived and designed the experiments; Contributed reagents, materials, analysis tools or data; Wrote the paper.

Bindesh Kumar Shukla: Performed the experiments; Analyzed and interpreted the data; Wrote the paper.

Funding statement

Umesh Yadava was supported by the Department of Science and Technology, New Delhi, India through the FAST Track Young Scientist Scheme (Ref. No. SR/FT/CS-78/2010).

Competing interest statement

The authors declare no conflict of interest.

Additional information

No additional information is available for this paper.

References

[1] S.L. Stanley Jr., Amoebiasis, Lancet 361 (2003) 1025.
[2] S. Marion, N. Guillén, Genomic and proteomic approaches highlight phagocytosis of living and apoptotic human cells by the parasite Entamoeba histolytica, Int. J. Parasitol. 36 (2006) 131.
[3] J.P. Ackers, D. Mirelman, Progress in research on entamoeba histolytica pathogenesis, Curr. Opin. Microbiol. 9 (2006) 367.
[4] S.L. Stanley, Pathophysiology of amoebiasis, Trends Parasitol. 17 (2001) 280.
[5] W.A. Petri Jr., Therapy of intestinal protozoa, Trends Parasitol. 19 (2003) 523.
[6] A.F. El-Nahas, I.M. El-Ashmawy, Reproductive and cytogenetic toxicity of metronidazole in male mice, Basic Clin. Pharmacol. Toxicol. 94 (2004) 226.
[7] V. Purohit, A.K. Basu, Mutagenicity of nitroaromatic compounds, Chem. Res. Toxicol. 13 (2000) 673.
[8] P. Abboud, V. Lemée, G. Gargala, P. Brasseur, J.J. Ballet, F. Borsa-Lebas, Successful treatment of metronidazole- and albendazole-resistant giardiasis with nitazoxanide in a patient with acquired immunodeficiency syndrome, Clin. Infect. Dis. 32 (2001) 1792.
[9] F. Hayat, A. Salahudin, S. Ummar, A. Azam, Synthesis, characterization, antiamoebic activity and cytotoxicity of novel series of pyrazoline derivatives bearing quinoline tail, Eur. J. Med. Chem. 45 (2010) 4669.
[10] A. Budakoti, M. Abid, A. Azam, Syntheses, characterization and in vitro antiamoebic activity of New Pd(II) complexes With 1-N-substituted thiocarbamoyl-3,5-diphenyl-2-pyrazoline Derivatives, Eur. J. Med. Chem. 42 (2007) 544.
[11] H. Parveen, F. Hayat, S. Mukhtar, A. Salahudin, A. Khan, F. Islam, A. Azam, Synthesis, characterization and Biological evaluation of novel 2,4,6-trisubstituted bis-pyrimidine derivatives, Eur. J. Med. Chem. 46 (2011) 4669.
[12] S.M. Siddiqui, A. Salahudin, A. Azam, Synthesis, characterization and antiamoebic activity of some hydrazone and azole derivatives bearing pyridyl moiety as a promising heterocyclic scaffold, Med. Chem. Res. 22 (2013) 775.
[13] U. Yadava, B.K. Shukla, M. Roychoudhury, D. Kumar, Pyrazolo[3,4-d]pyrimidines as novel inhibitors of O-acetyl-L-serine sulfhydrylase of entamoeba histolytica: an in silico study, J. Mol. Model. 21 (2015) 96.
[14] U. Yadava, M. Singh, M. Roychoudhury, Pyrazolo[3,4-d]pyrimidines as inhibitor of anti-coagulation and inflammation activities of phospholipase A_2: insight from molecular docking studies, J. Biol. Phys. 39 (2013) 419.
[15] U. Yadava, B.K. Shukla, M. Roychoudhury, Pyrazolo [3, 4-d] pyrimidines as the inhibitors of mycobacterial β-oxidation trifunctional enzyme, Med. Chem. Res. 24 (2015) 4002.
[16] A.A. Bekhit, T. Abdel-Azeim, Design, synthesis and biological evaluation of some pyrazole derivatives as anti-inflammatory-antimicrobial agents, Bioorg. Med. Chem. 12 (2004) 1935.
[17] G.B. Elion, S.W. Callahan, H. Nathan, S. Bieber, R.W. Rundles, G.H. Hilching, Potentiation by inhibition of drug degradation : 6-substituted purines and xanthine oxidase, Biochem. Pharmacol. 12 (1963) 85.
[18] S. Schenone, C. Brullo, F. Musumeci, M. Botta, Novel dual Src/Abl inhibitors for hematologic and solid malignancies, Expet Opin. Invest. Drugs 19 (2010) 931.
[19] U. Yadava, M. Singh, M. Roychoudhury, Gas-phase conformational and intramolecular p–p interaction studies on somepyrazolo[3,4-d]pyrimidine derivative, Comput. Theo. Chem. 977 (2011) 134.
[20] K. Avasthi, D. Bhagat, C. Bal, A. Sharon, U. Yadava, P.R. Maulik, Unusual molecular conformationin dissymmetric propylene-linkercompounds containing pyrazolo-[3,4-d]pyrimidine and phthalimidemoieties, Acta Crystallogr. C59 (2003) o409.
[21] M. Arivazhagana, J.S. Kumar, Vibrational analysis of 4-amino pyrazolo (3,4-d) pyrimidine a joint FTIR, laser Raman and scaled quantum mechanical studies, Spectrochim. Acta, Part A 82 (2011) 228.
[22] M.J. Frisch, et al., GAUSSIAN 03 Revision B.04, Gaussian Inc Pittsburgh, 2003.
[23] B.K. Shukla, U. Yadava, M. Roychoudhury, Theoretical explorations on the molecular structure and IR frequencies of 3-phenyl-1-tosyl-1H-pyrazolo[3,4-d] pyrimidin-4-amine in view of experimental results, J. Mol. Liq. 212 (2015) 325.
[24] S.H. Vosco, L. Wilk, M. Nusair, Accurate spin-dependent electron liquid correlation energies for local spin density calculations: a critical analysis, Can. J. Phys. 1200 (1980).
[25] J.M. Campanario, E. Bronchalo, M.A. Hidalgo, An effective approach for teaching intermolecular interactions, J. Chem. Educ. 71 (1994) 761.
[26] I. Raj, M. Mazumdar, S. Gaurinath, E. histolytica: insights from structural and molecular dynamics simulation studies, Biochim. Biophys. Acta 1830 (2013) 4573.
[27] Glide: Version 5.2, Schrödinger. LLC, New York, 2012.
[28] M. Arivazhagan, J.S. Kumar, Vibrational assignment, HOMO – LUMO, first-hyperpolarizability and Mulliken's charge analysis of 2,7-dinitrofluorene, Indian J. Pure Appl. Phys. 50 (2012) 363.
[29] U. Yadava, S.K. Yadav, R.K. Yadav, Electronic structure, vibrational assignments and simulation studies withA/T rich DNA duplex of an aromatic bis-amidine derivative, DNA Repair 60 (2017) 9–17.
[30] R.S. Mulliken, Electronic population analysis on LCAO–MO molecular wave functions. I, J. Chem. Phys. 231 (1955) 833.
[31] C.Y. Liang, F.G. Pearson, R.H. Marchessault, The tertiary CH and CD vibrational frequencies in polyacrylonitrile and α-deutero polyacrylonitrile, Spectrochim. Acta 17 (1961) 568.
[32] B.K. Sharma, Molecular *Spectroscopy*, 11, Goel Publishing House, Meerut, 1995.
[33] QikProp: Version 3.5, Schrödinger LLC, New York, 2012.